Human Reproduction Vol.23, No.9 pp. 1983–1992, 2008 doi:10.1093/humrep/den206
Advance Access publication on June 7, 2008

Quantitative morphometrical characterization of human pronuclear zygotes

A. Beuchat[1], P. Thévenaz[1], M. Unser[1], T. Ebner[2], A. Senn[3], F. Urner[3], M. Germond[3] and C.O.S. Sorzano[4,5]

[1]Biomedical Imaging Group, Swiss Federal Institute of Technology Lausanne, Lausanne, Switzerland; [2]Women's General Hospital, IVF-Unit, Linz, Austria; [3]Fondation F.A.B.E.R & Centre of Medically Assisted Procreation, Lausanne, Switzerland; [4]Department of Electronic and Telecommunication Systems, University of San Pablo — CEU, Campus Urb. Montepríncipe s/n, 28668 Boadilla del Monte, Madrid, Spain

[5]Correspondence address. E-mail: coss.eps@ceu.es

BACKGROUND: Identification of embryos with high implantation potential remains a challenge in *in vitro* fertilization (IVF). Subjective pronuclear (PN) zygote scoring systems have been developed for that purpose. The aim of this work was to provide a software tool that enables objective measuring of morphological characteristics of the human PN zygote. METHODS: A computer program was created to analyse zygote images semi-automatically, providing precise morphological measurements. The accuracy of this approach was first validated by comparing zygotes from two different IVF centres with computer-assisted measurements or subjective scoring. Computer-assisted measurement and subjective scoring were then compared for their ability to classify zygotes with high and low implantation probability by using a linear discriminant analysis. RESULTS: Zygote images coming from the two IVF centres were analysed with the software, resulting in a series of precise measurements of 24 variables. Using subjective scoring, the cytoplasmic halo was the only feature which was significantly different between the two IVF centres. Computer-assisted measurements revealed significant differences between centres in PN centring, PN proximity, cytoplasmic halo and features related to nucleolar precursor bodies distribution. The zygote classification error achieved with the computer-assisted measurements (0.363) was slightly inferior to that of the subjective ones (0.393). CONCLUSIONS: A precise and objective characterization of the morphology of human PN zygotes can be achieved by the use of an advanced image analysis tool. This computer-assisted analysis allows for a better morphological characterization of human zygotes and can be used for classification.

Keywords: zygote; *in vitro* fertilization; image analysis; morphometrical characterization

Introduction

In vitro fertilization (IVF) is a common technique in medically assisted reproduction that has been continuously improved during the last few decades. Despite progress in the IVF technique itself, only a minority of the *in vitro*-generated embryos have the ability to implant and to give a viable pregnancy, probably because of intrinsic characteristics of the gametes. To increase the probability of implantation, several embryos are usually transferred at the same time in each patient. The drawback of this practice is a high frequency of multiple pregnancies that often lead to dramatic health and economic problems. To avoid multiple pregnancies and to guarantee high pregnancy rates, the transfer of a single embryo with high implantation potential would be the ideal strategy.

Identifying embryos with high implantation potential remains a challenge in IVF and different approaches have been adopted for that purpose. The most widely supported strategy to choose viable embryos is to rely on the number of blastomeres and the grade of the embryos at the time of embryo transfer. However, these morphological aspects do not correlate sufficiently with the embryonic viability to allow a univocal microscopic recognition of the embryos able to produce a viable pregnancy. A number of other strategies have thus been proposed to improve the prognostic evaluation of embryo viability, including selection of early cleaving embryos (Shoukir *et al*., 1997), culture up to the blastocyst stage (Gardner *et al*., 1998) and scoring of pronuclear (PN) stage zygotes (Ebner *et al*., 2003). Unfortunately, legal constraints in some countries prevent the use of approaches involving embryo selection. In Switzerland, identification of potentially viable embryos is thus limited either to oocytes prior to fertilization or to PN stage zygotes (Germond and Senn, 1999).

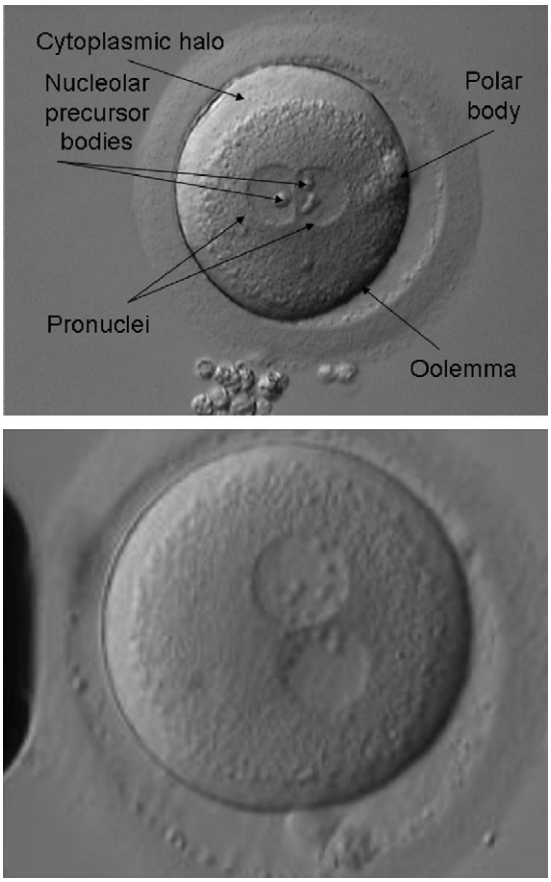

Figure 1: Images of human pronuclear stage zygotes of Group I (top) and Group II (bottom).

Several features of the PN zygotes (see Fig. 1), including the cytoplasmic halo, the position of the PN and the number and distribution of nucleolar precursor bodies (NPB) in PN, have been proposed as indicators of embryo viability and chromosomal normality (Garello *et al*., 1999; Tesarik and Greco, 1999; Scott *et al*., 2000; Senn *et al*., 2006; Gianaroli *et al*., 2007). PN zygote scoring systems have been developed, focusing on a single or on a series of features, but all having in common a subjective microscopic observation of zygotes. No study has so far specifically attempted to evaluate the contribution of morphological characteristics automatically detected by an advanced image analysis tool. The aim of the present study was to provide a software tool that enables objective measuring of morphological characteristics, which may be used as possible markers of future embryo developmental competence. For that purpose, an ImageJ plug-in was created that allows the measurement of a large number of morphometrical features of the human PN zygote.

Materials and Methods

Patients

Patients undergoing IVF (or ICSI) treatments at the Centre of Medically Assisted Reproduction in Lausanne (Group I) and at the Women's General Hospital in Linz (Group II) were included in this study (Table I). For both groups, all the patients of consecutive IVF or ICSI cycles occurring during a 6 month period were retained, without any patient selection. Due to national legal constraints, the embryo selection strategy was different between the two groups. For Group I, 1–3 PN zygotes were randomly allocated for transfer after fertilization assessment, while all the others were immediately frozen. For Group II, all zygotes were cultured until transfer on Day 2 or 3, and 1–3 of the best embryos were chosen for transfer.

Table I. Zygotes from Groups I and II.

	Group I	Group II
Number of patients	98	112
Age, Mean ± SD	36.5 ± 4.1	33.3 ± 4.4
Number of transferred embryos	188	201
Number of implanted embryos (%)	28 (14.8)	62 (30.8)
Number of pregnancies (%)	27 (27.5)	53 (47.3)
Number of zygote images[a]	188	201

[a]All the zygote images corresponded to the transferred embryos.

Another group of 107 patients from Group III, for whom all transferred zygotes ($n = 206$) had a known implantation outcome, was used for a zygote classification test (see classification of zygotes). In this group, all the implanted zygotes ($n = 84$) originated from single or twin pregnancies after the transfer of one or two embryos, respectively. Embryos were considered as implanted when a gestational sac with fetal heartbeat was observed by ultrasound, 5–6 weeks after embryo transfer.

Image acquisition

Zygotes were observed at the PN stage 17–20 h after insemination under an inverted microscope equipped with a Hoffman modulation contrast (Hoffman and Gross, 1970; Murphy, 2001). An Octax Eyeware camera (Octax, MTG, Herborn, Germany) attached to the microscope was used to acquire zygote digital images that were then stored in the Eyeware database until image processing. Images of PN zygotes with different magnification (Fig. 1) were provided by the Centre of Medically Assisted Reproduction in Lausanne (201 images) and by Dr T. Ebner from the General Woman Hospital in Linz (188 images). All the photographed zygotes analysed in this study corresponded to the transferred embryos.

Image processing

Photographed zygotes were subjectively scored according to Senn *et al*. (2006) and objectively analysed by using the computer-assisted method.

In subjective scoring, scores were assigned to the six following parameters: centring of the two PN, proximity of PN, orientation of PN with respect to polar bodies, number of NPB, polarization of NPB and cytoplasmic halo. Scores ranged from 1 (worst) to 3 (best). A cumulated pronuclear score, ranging from 6 to 18, was obtained by adding the six individual scores.

In the computer-assisted method, a plug-in of the image processing ImageJ (http://rsb.info.nih.gov/ij) was created in Java programming language to quickly analyse zygote digital images and to minimize subjectivity (the plug-in accessible from http://biolab.uspceu.com/recursos.php). We developed a sequence of image-processing steps leading to the measurement of 24 morphological features related to the six characteristics pointed out by Senn *et al*. (2006). Our image-processing steps can be visualized in Fig. 2 and are briefly summarized as follows:

- Automatic detection of the oolemma
- Semi-automatic detection of the cytoplasmic halo
- NPB manual selection

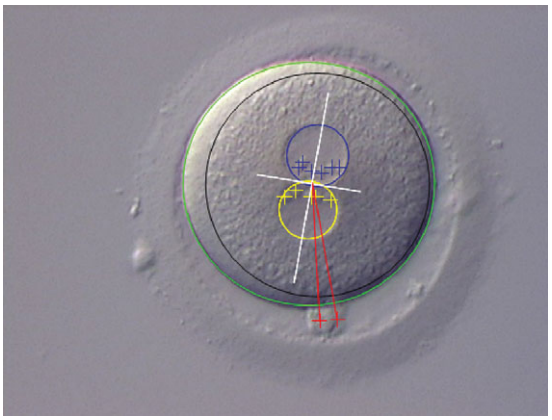

Figure 2: Computer-dependent measurements of morphological features in zygotes.
The oolemma (green) and cytoplasmic halo (black) ellipses have been drawn as well as the pronuclei circles and nucleolar precursor bodies (blue and yellow). The axis defined by the two PN has been also drawn (white) together with the line separating the two PN (white). The red lines join the two polar bodies with the centre of the white cross.

- Semi-automatic detection of PN
- Polar bodies manual selection
- Morphological measurements

Automatic detection of the oolemma
The oolemma detection was performed in several steps:

Foreground detection. First, the region with the central oocyte is separated from the background. For this, we perform a segmentation by region on the basis of the four image corners. We assume that each corner belongs to the image background and is characteristics of a region when $[(I(x.y) - \hat{\mu})/s] < 0.1$, where $I(x,y)$ is the image pixel being considered, $\hat{\mu}$ is the current estimate of the mean grey value for this region and s is the current estimate of SD of the grey values within the region. Each time a pixel is accepted as belonging to the region, the statistical estimates are updated. The four regions are considered to belong to the background of the image, whereas the rest of the pixels are considered to be the foreground containing the oolemma. The pixels in the border between the foreground and the background are selected and an ellipse is fitted to these pixels as suggested by Fitzgibbon *et al*. (1999). The Hough transform (Illingworth and Kittler, 1988) could have been used in order to find the best fitting ellipse. However, the computational cost of the Hough transform exceeds that of the algorithm proposed by Fitzgibbon. Figure 3 shows the result of this foreground detection. Note that if one of the corners is occupied by another oocyte, it does not hinder the right detection of an ellipse within which the oolemma lies. Next, the smallest rectangular image enclosing the foreground ellipse is computed and from this point on, all operations are applied to this sub image.

Oolemma boundary detection. The second step is to automatically detect the pixels belonging to the boundary of the oolemma. For this, we apply a Gaussian blur of radius 2 pixels, and then a Sobel edge filter. We then binarize using a Lloyd–Max classification with two classes, morphologically close the image with a square structure element of two pixels, compute the skeleton of the result, and finally suppress small blobs by dilating with a square structure element of one pixel. Figure 4 shows this process.

Figure 3: Detection of an ellipse (foreground) where the studied oolemma lies.

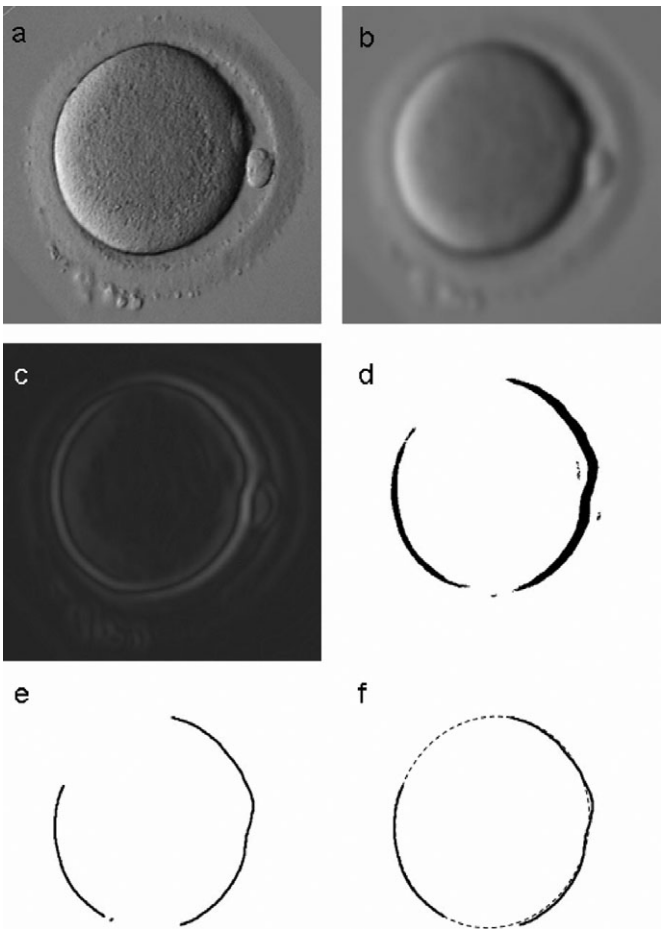

Figure 4: Detection of oolemma boundary pixels.
(**a**) original oocyte; (**b**) oocyte after Gaussian blurring; (**c**) oocyte after Sobel filtering; (**d**) oolemma edges obtained by Lloyd–Max classification and morphological closure; (**e**) oolemma edges after skeletonization; (**f**) oolemma edges after blob suppression (the ellipse fitted to the oolemma is shown as a dashed line in this image).

Oolemma approximation by an ellipse. Finally, an ellipse is fitted (Fitzgibbon *et al*., 1999) to the oolemma boundary pixels. The bottom-right image of Fig. 4 shows the fitted ellipse as a dashed line.

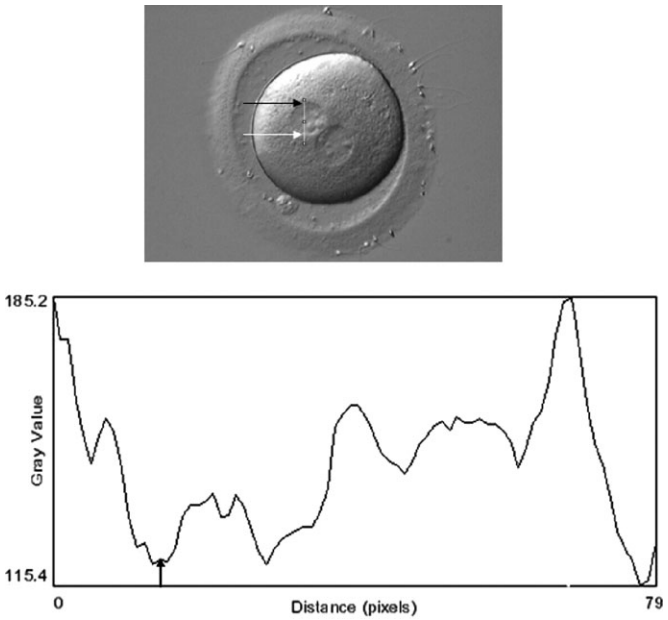

Figure 5: Profile of the grey values along a line in one pronucleus. It can be seen that along this line one of the borders is a local minimum (dark border), while the other border is a local maxima (bright border). Just in the transition between dark and bright borders, there is a region where the border is of the same intensity as its background.

Semi-automatic detection of the cytoplasmic halo

The cytoplasmic halo is semi-automatically computed with the help of a few points (at least 5) selected by the user on the border of the cytoplasmic retraction. An ellipse is fitted to these selected points (Fitzgibbon *et al*., 1999). An example of the detection of the cytoplasmic halo is shown in Fig. 2 as a black ellipse.

NPB manual selection

NPBs are small spots within the PN. These are very difficult to detect correctly and robustly over a wide range of images. This task requires significant training and is completely left to the user who must select them within the image. Furthermore, the NPB positions are used in the next step for constraining the search of the PN. For this reason, we call the next step a semi-automatic detection.

PN semi-automatic detection

PN pose two difficulties for correct identification: first, their borders are faint and sometimes overlap; second, due to the Hoffman modulation, along the PN border there are bright pixels, dark pixels and pixels of the same greyness as their background (see Fig. 5). However, semi-automatic detection is possible by applying the following image-processing steps and the knowledge of the NPB positions:

Light correction. The direction of light is calculated using the inertia matrix.

$$M(x,y)=\begin{pmatrix} \sum_{x,y} 2|\nabla I(x,y)|\cos^2(\alpha(x,y)) & \sum_{x,y} 2|\nabla I(x,y)|\cos(\alpha(x,y)\sin(\alpha(x,y)) \\ \sum_{x,y} 2|\nabla I(x,y)|\cos(\alpha(x,y)\sin(\alpha(x,y)) & \sum_{x,y} 2|\nabla I(x,y)|\sin^2(\alpha(x,y)) \end{pmatrix},$$

where

$$\alpha(x,y)=\arctan\left(\frac{\partial I(x,y)/\partial y}{\partial I(x,y)/\partial x}\right) \text{ and } \nabla I(x,y)=\left(\frac{\partial I(x,y)}{\partial x},\frac{\partial I(x,y)}{\partial y}\right).$$

Derivatives are computed using cubic spline interpolation as described by Unser *et al*. (1993). The signs of the image gradient components help to disambiguate the quadrant of the gradient angle. In practice, the partial derivatives $\partial I(x,y)/\partial x$ and $\partial I(x,y)/\partial y$ are convolved with a Gaussian whose SD is 3 in order to avoid instabilities in the derivative estimation due to image noise.

Calling m_{ij} to the ij-th component of the inertia matrix, the angle of the light can be computed as.

$$\beta=\frac{2\,m_{01}}{m_{00}-m_{11}+\sqrt{4\,m_{01}^2+(m_{00}-m_{11})^2}}$$

Once the light direction is detected, the image is rotated so that the light comes from the vertical direction. The rotated image is then filtered vertically with a band pass filter whose transfer function is.

$$H(z)=\frac{\alpha(z-z^{-1})}{\alpha z-(1+\alpha^2)+\alpha z^{-1}},$$

where $\alpha = 0.98$ (this value has been determined empirically).

The resulting band pass filtered image is rotated back β degrees. The output of this process is an image where the differences in illumination due to the Hoffman modulation are negligible. The PN are automatically sought in this light-corrected image. It can be seen in Fig. 6 that the PN limits are darker than their surroundings in this light-corrected image.

PN detection. The finding of the two PN is performed on the light-corrected image in a number of steps:

(i) Histogram equalization (Jain, 1989, Chap. 7).
(ii) Blurring with a Gaussian kernel with a SD of 5.

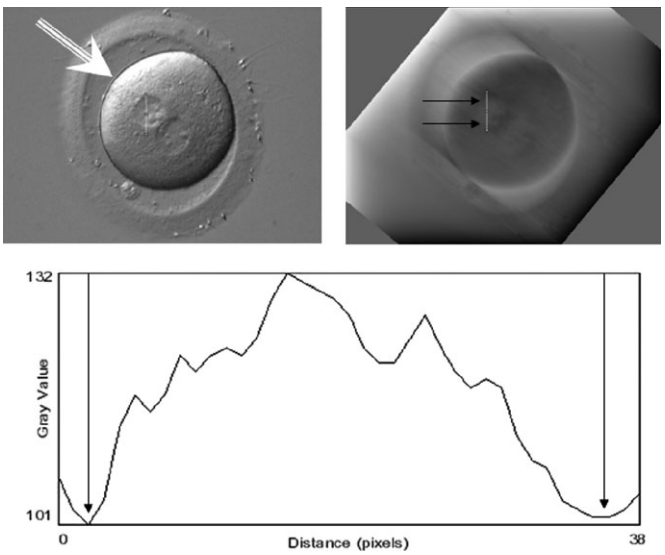

Figure 6: Left: original oocyte with a thick arrow pointing the light direction as created by the Hoffman modulation.
(Right) Oocyte after the upwards filtering (two black arrows point the limits of the PN). (Bottom) Intensity profile of the light corrected image where the two black arrows indicate the limits of the PN.

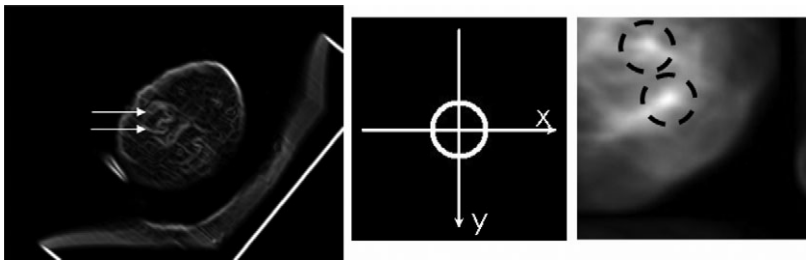

Figure 7: (Left) Edge image after histogram equalization and Gaussian blurring of the light-corrected image in Fig. 6. (Middle) Template used for the correlation computation, the template models the PN border and its radius is varied within a range that includes 13 and 14 μm. (Right) The position of the two correlation maxima have been encircled by a dash line).

(iii) Edge finding using a Sobel operator. The result of this step and the previous two on the light-corrected image is shown in Fig. 7 (left).
(iv) The edge image is correlated to a family of PN edge templates. These templates are produced knowing that the human PN radius is of a size between 13 and 14 μm. Using the image sampling rate, this size range translates into a size range expressed in pixels. There is a PN edge template for every circle with integer radius within this latter range. The correlation between the edge image and each of the templates is computed, and for each pixel the maximum correlation with all possible templates is kept. The resulting image is referred to as the maximum correlation image, and is also shown in Fig. 7 (right).
(v) The centre of the two PN is sought as the maximum correlation peaks found within a distance of 13 μm around the corresponding sets of NPBs (previously manually marked by the user).

Polar bodies manual selection

As for the NPBs, the identification of polar bodies is not easily automated with 100% reliability. However, a trained embryologist can simply tell the program whether the two polar bodies are visible, only one is visible or none. When they are seen, the user must indicate their position.

Morphological measurements

Once the different morphological features of the zygotes have been detected (automatically, semi-automatically or manually), we associate a 27-dimensional feature vector to each zygote. The first three components of this vector are input by the user and they relate to the zygote treatment (fertilization method and preservation state) and the presence or absence of polar bodies. The following 24 components are computed from the morphological characterization described in previous sections. As exemplified in Fig. 2, these computed components largely remove the subjectivity introduced in the zygote scoring scheme previously proposed by Senn *et al*. (2006).

Classification of zygotes

Zygotes belong to two classes, representing zygotes with low and high implantation probability, respectively. Zygotes of Group III were assigned to either class by using linear discriminant analysis (LDA) after subjective scoring and computer-assisted measurements. LDA is a classification technique (Webb, 2002) that, given a feature vector $\mathbf{x}$ (in the case of the vector of subjective scores), aims at classifying it in one of two classes (in our case, the classes of zygotes with high and low implantation chances respectively). This is done with the help of a linear function $h(\mathbf{x}) = \mathbf{wx} = w_0$, where $\mathbf{w}$ is a weight vector, and w_0 is a threshold. If, for a given $\mathbf{x}$, $h(\mathbf{x}) < 0$, then it is classified as belonging to class of low implantation probability; while if $h(\mathbf{x}) \geq 0$, then it is classified as belonging to the class of high implantation probability. In the scheme proposed in Senn *et al*. (2006), a decision rule was proposed based on the accumulated experience that zygotes with a score of 15 or larger had more chances to successfully implant. From a classification point of view, this decision rule corresponds to a LDA with $\mathbf{w} = (1,1,...,1)^t$ and $w_0 = -15$. Error rates of classification were determined by using *k*-fold cross validation when either subjective scoring or computer-assisted objective measurements were used to characterize zygotes.

Statistical tests

The non-parametric Mann–Whitney *U* test was used to test whether different groups of measures were drawn from the same distribution (*P*-values of this test are shown in Tables II, III and IV). Student's *t*-test was used to compare error rates of classification. Differences were considered as significant when $P < 0.05$.

Results

According to Senn *et al*. (2006), zygotes were scored 1, 2 or 3, for the following six features: centring of the PN, proximity of the PN, orientation of the PN in respect to the polar bodies, total number of NPB, polarization of NPB and cytoplasmic halo. Zygotes were also subjected to the computer-assisted method proposed in this article. The same observer in Group I scored all zygotes. Figs 8–13 show images of subjectively scored zygotes and their corresponding objective measurements by using the ImageJ plug-in. While subjective scoring is global for each of the six features, the computer-assisted analysis associates several measurements to each parameter.

Comparison of the measurement of distances for zygotes coming from two different centres

To validate the use of the plug-in on a larger scale, we analysed two groups of zygote images coming from two different IVF

Table II. Objective measurements of the size of zygotes and their pronuclei.

Feature	Group I ($n = 188$)	Group II ($n = 201$)	*P*-value
Zygote size			
Major axis (μm)	56.3 ± 2.9	56.0 ± 2.7	0.51
Minor axis (μm)	54.0 ± 2.7	54.3 ± 3.2	0.41
Pronucleus size			
Radius pronucleus 1 (μm)	12.5 ± 0.9	12.6 ± 0.8	0.10
Radius pronucleus 2 (μm)	12.2 ± 0.9	12.1 ± 0.9	0.60
Relative radius pronucleus 1	0.22 ± 0.02	0.22 ± 0.02	0.34
Relative radius pronucleus 2	0.22 ± 0.02	0.21 ± 0.02	0.49

Table III. Groups I and II: subjective scoring (bold features, $n = 6$) and computer-assisted measurements ($n = 24$) of PN centring, PN proximity, PN orientation, number of NPB, distribution of NPB and cytoplasmic halo.

Feature	Group I, ($n = 188$)	Group II, ($n = 201$)	*P*-value
1. PN centring	**2.4 ± 0.6**	**2.3 ± 0.7**	**0.22**
2. Centring (μm)	12.3 ± 3.1	13.8 ± 3.3	0.00
3. Relative centring	0.22 ± 0.06	0.25 ± 0.06	0.00
4. PN proximity	**2.4 ± 0.6**	**2.3 ± 0.7**	0.19
5. Proximity (μm)	20.8 ± 3.4	23.1 ± 3.0	0.00
6. Relative proximity	0.8 ± 0.1	0.9 ± 0.1	0.00
7. PN orientation	**2.1 ± 0.6**	**2.0 ± 0.63**	**0.06**
8. Angle closest polar body (rad)	0.6 ± 0.5	0.8 ± 0.5	0.11
9. Angle farthest polar body (rad)	0.7 ± 0.5	0.8 ± 0.6	0.42
10. Sum of angles (rad)	1.4 ± 0.9	1.6 ± 1.0	0.19
11. Number of NPB	**2.4 ± 0.7**	**2.3 ± 0.7**	**0.49**
12. Number of NPB pronucleus 1	6.7 ± 0.9	7.0 ± 2.3	0.23
13. Number of NPB pronucleus 2	4.5 ± 1.5	4.4 ± 1.5	0.17
14. Sum	11.2 ± 3.0	11.4 ± 3.3	0.82
15. Difference, number of NPB	2.2 ± 1.7	2.7 ± 2.1	0.01
16. NPB polarization	**1.9 ± 0.6**	**2.0 ± 0.6**	**0.054**
17. Centre of gravity pronucleus 1 (μm)	5.9 ± 1.23	5.8 ± 1.4	0.35
18. Centre of gravity pronucleus 2 (μm)	5.1 ± 1.4	4.5 ± 1.3	0.00
19. Regression pronucleus 1 (μm)	3.2 ± 1.2	3.0 ± 1.4	0.04
20. Regression pronucleus 2 (μm)	2.6 ± 1.4	1.9 ± 1.1	0.00
21. Splitting pronucleus 1 (μm)	7.5 ± 2.3	7.9 ± 2.1	0.20
22. Splitting pronucleus 2 (μm)	6.7 ± 2.1	6.2 ± 1.9	0.02
23. Cytoplasmic halo	**2.2 ± 0.8**	**1.9 ± 0.8**	**0.00**
24. Retracted cytoplasm surface	0.79 ± 0.08	0.84 ± 0.08	0.00
25. Major axis (μm)	50.5 ± 3.0	52.1 ± 4.9	0.00
26. Minor axis (μm)	47.7 ± 3.3	48.8 ± 4.7	0.00
27. Axis ratio	1.06 ± 0.06	1.05 ± 0.16	0.58
28. Shift (rad)	1.0 ± 0.9	0.9 ± 0.89	0.63
29. Centring (μm)	4.2 ± 2.1	3.3 ± 2.2	0.00
30. Relative centring	0.08 ± 0.04	0.06 ± 0.09	0.00

Table IV. Group III: subjective scoring (bold features, $n = 6$) and computer-assisted measurements ($n = 24$) of PN centring, PN proximity, PN orientation, number of NPB, distribution of NPB and cytoplasmic halo.

Feature	Implanted zygotes ($n = 84$)	Non-implanted zygotes ($n = 122$)	*P*-value
1. PN centring	**2.27 ± 0.63**	**2.27 ± 0.59**	**0.98**
2. Centring (μm)	12.08 ± 3.4	11.95 ± 3.19	0.93
3. Relative centring	0.21 ± 0.062	0.22 ± 0.058	0.43
4. PN proximity	**1.75 ± 0.44**	**1.81 ± 0.39**	**0.29**
5. Proximity (μm)	20.66 ± 5.1	20.09 ± 4.59	0.317
6. Relative proximity	0.85 ± 0.22	0.84 ± 0.18	0.676
7. PN orientation	**1.94 ± 0.55**	**2.07 ± 0.62**	**0.109**
8. Angle closest polar body (rad)	0.75 ± 0.51	0.58 ± 0.51	0.087
9. Angle farthest polar body (rad)	0.97 ± 0.64	0.80 ± 0.58	0.015
10. Sum of angles (rad)	1.78 ± 0.98	1.49 ± 0.93	0.046
11. Number of NPB	**2.06 ± 0.63**	**2.0 ± 0.65**	**0.57**
12. Number of NPB pronucleus 1	6.13 ± 1.91	5.5 ± 1.7	0.008
13. Number of NPB pronucleus 2	3.75 ± 1.43	4.10 ± 1.25	0.013
14. Sum	9.88 ± 2.83	9.61 ± 2.64	0.642
15. Difference, number of NPB	2.38 ± 1.82	1.4 ± 1.4	0000
16. NPB polarization	**1.75 ± 0.64**	**1.61 ± 0.65**	**0.094**
17. Centre of gravity pronucleus1 (μm)	5.63 ± 1.4	5.61 ± 1.21	0.57
18. Centre of gravity pronucleus 2 (μm)	4.67 ± 1.42	5.11 ± 1.24	0.140
19. Regression pronucleus 1 (μm)	3.43 ± 1.51	3.26 ± 1.21	0.52
20. Regression pronucleus 2 (μm)	2.45 ± 1.32	3.06 ± 1.80	0.007
21. Splitting pronucleus 1 (μm)	7.56 ± 2.87	7.95 ± 2.69	0.174
22. Splitting pronucleus 2 (μm)	7.14 ± 2.94	7.75 ± 2.72	0.068
23. Cytoplasmic halo	**2.02 ± 0.67**	**2.05 ± 0.68**	**0.72**
24. Retracted cytoplasm surface (%)	74.11 ± 7.083	74.62 ± 6.62	0.44
25. Major axis (μm)	49.25 ± 2.94	48.36 ± 3.46	0.089
26. Minor axis (μm)	45.65 ± 1.87	44.62 ± 3.27	0.015
27. Axis ratio	1.075 ± 0.056	1.08 ± 0.075	0.232
28. Shift (rad)	0.885 ± 0.806	0.9540.88	0.71
29. Centring (μm)	3.59 ± 2.01	1.92 ± 1.77	0.012
30. Relative centring	0.075 ± 0.042	0.063 ± 0.039	0.035

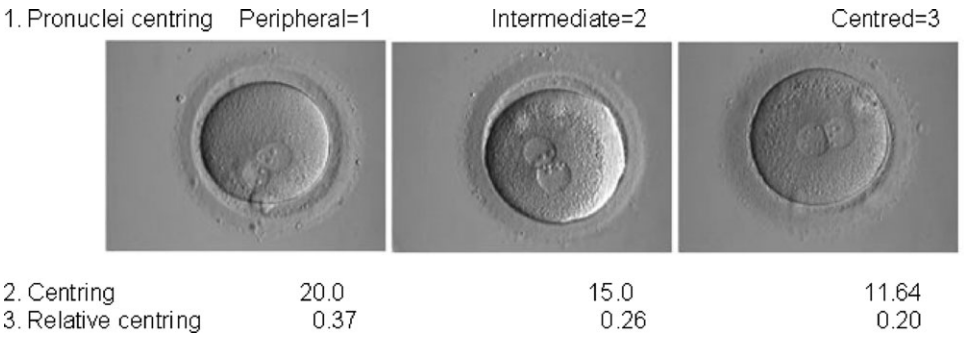

Figure 8: (1) Centring of the PN.
Computer-assisted measurements: (2) Centring: absolute distance (μm) between zygote centre and the PN barycentre; (3) Relative centring: centring/zygote radius.

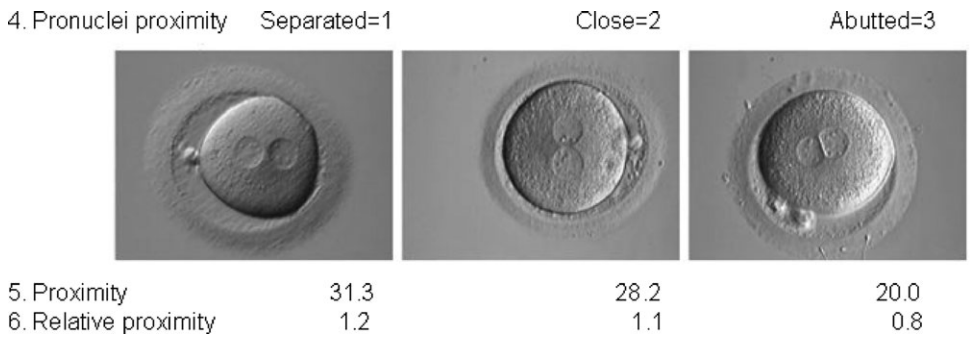

Figure 9: (4) Proximity of the PN.
Computer-assisted measurements: (5) Proximity: absolute distance (μ m) between the two centres of the PN; (6) Relative proximity: proximity/Sum of the PN radii.

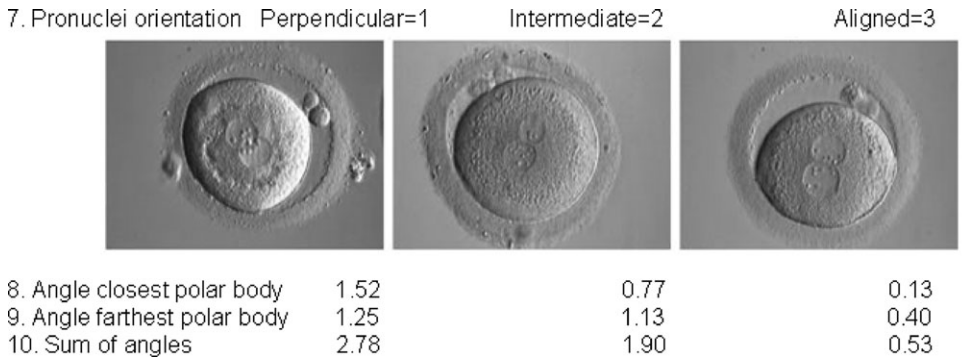

Figure 10: (7) Orientation of the PN according to the polar bodies.
Computer-assisted measurements: (8) Angle closest polar body (radians): angle between the PN axis and the closest polar body; (9) Angle farthest polar body (radians): angle between the PN axis and the farthest polar body; (10) Sum of the previous two angles (radians).

centres (Lausanne and Linz). The plug-in succeeded in analysing all images coming from these two centres. Precise measurements of zygote and pronucleus sizes were provided by the plug-in. The distribution of the size of the zygotes and their PN was found to be statistically similar in zygotes coming from both centres (Table II).

Comparison of the computer-assisted measurements versus the subjective scores

As shown in Table III, computer-assisted measurement and subjective scoring were first compared between PN zygotes from Group I and Group II. When subjectively scored, PN centring and proximity were not significantly different between the two groups, but a significant difference was observed when these parameters were objectively measured. PN orientation according to the polar bodies was similar in both groups when assessed either with subjective scoring or computer-assisted measurement. NPB numbers were similar, but the difference in NPB number between pronucleus 1 (the pronucleus with the highest number of NPB) and pronucleus 2 (the other pronucleus), calculated only by the plug-in, was significantly higher in the Group II. Concerning NPB polarization, a non-significant ($P = 0.054$)

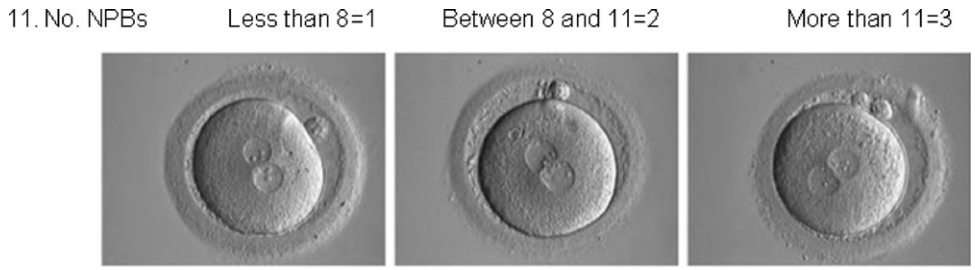

12. No. NPB pronucleus 1	4	6	7
13. No. NPB pronucleus 2	3	3	6
14. Sum No. NPB	7	9	13
15. Difference No. NPB	1	3	1

Figure 11: (11) Number of nucleolar precursor bodies.
Computer-assisted measurements: (12) Number of NPBs in the pronucleus with more NPBs; (13) Number of NPBs in the pronucleus with fewer NPBs; (14) Total number of NPBs in the two PN; (15) Difference in the number of NPBs between the two PN.

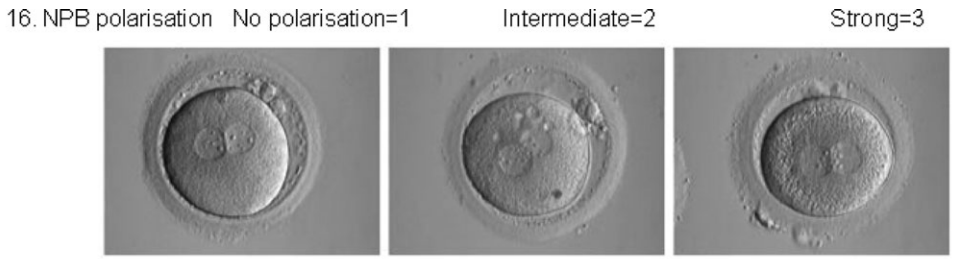

17. Centre of gravity pronucleus 1	7.4	6.5	5.2
18. Centre of gravity pronucleus 2	6.2	6.6	5.4
19. Regression pronucleus 1	4.6	3.5	2.7
20. Regression pronucleus 2	4.5	5.3	1.8
21. Splitting pronucleus 1	13.4	7.2	4.7
22. Splitting pronucleus 2	9.2	9.7	6.3

Figure 12: (16) Distribution of NPB inside the PN.
Computer-assisted measurements: (17) Centre of gravity pronucleus 1: mean distance (μm) between the NPBs and their gravity centre in pronucleus1; (18) Similar measure for pronucleus 2; (19) Regression pronucleus 1: mean distance (μm) between the NPBs and their regression line in pronucleus 1; (20) Similar measure for pronucleus 2; (21) Splitting pronucleus 1: mean distance (μm) between the NPBs and the line separating the two pronucleus; (22) Similar measure for pronucleus 2.

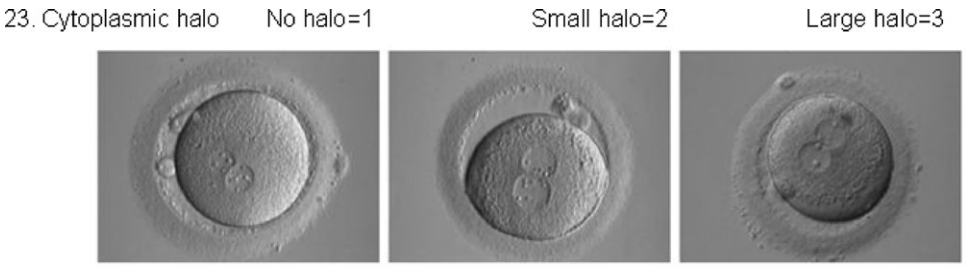

24. Retracted cytoplasm surface	0.81	0.77	0.72
25. Major axis	52.2	49.0	46.3
26. Minor axis	49.5	47.8	43.8
27. Axis ratio	1.05	1.02	1.05
28. Shift	0.22	0.22	0.16
29. Centring	3.8	3.5	7.46
30. Relative centring	0.07	0.07	0.16

Figure 13: (23) Cytoplasmic halo.
Computer-assisted measurements: (24) Retracted cytoplasm surface: ratio retracted cytoplasm surface/zygote surface; (25) Major axis (μm) of the retracted cytoplasm ellipse; (26) Minor axis of the same ellipse; (27) Axis ratio: major axis/Minor axis; (28) Shift (radians): angle between the major axis of the retracted cytoplasm ellipse and the major axis of the zygote ellipse; (29) Centring: absolute distance (μm) between the centre of the retracted cytoplasm and the centre of the zygote; (30) Relative centring: centring/retracted cytoplasm radius.

higher subjective score was observed in zygotes of Group II. Computer-assisted analysis revealed a significantly higher NPB polarization of pronucleus 2 in the Group II, as indicated by lower mean distances of NPB to their gravity point, to their regression line and to the line splitting the PN. In pronucleus 1, the only significant observation was a lower distance of NPB to their regression line in the Group II, suggesting less dispersed NPB in this pronucleus in zygotes of Group II. Subjective scoring showed a significantly smaller cytoplasmic halo in zygotes of the Group II that was confirmed by computer-assisted measurements. The two axes and the relative surface of the retracted cytoplasm were larger, resulting in lower size of the halo in the Group II. In addition the halo was significantly more centred in these zygotes.

Computer-assisted measurement and subjective scoring were then compared for their ability to classify zygotes with high and low implantation probability. Zygotes of Group III were used for this classification analysis (Table IV). In this group, the mean subjective scores of implanted zygotes were not significantly different from the non-implanted zygotes. In contrast, computer-assisted measurements evidenced significant differences between implanted and non-implanted zygotes concerning the number of NPB in PN1 and PN2, respectively, the distribution of NPB in PN2 (regression PN2) and the centring of the cytoplasmic halo.

The zygote scoring scheme previously proposed by Senn *et al*. (2006) computes the sum of all the subjective scores. If the sum is above 15, then the zygote is classified as having a high implantation probability. If the sum is below 15, then the zygote is classified as having a low implantation probability. In the present study, this approach resulted in a classification error of 0.398. If one looks for the optimal weight vector and threshold separating the class of zygotes with high implantation potential and the class of zygotes with low implantation potential using the same subjective data, a 10-fold cross validation experiment showed that the classification error of such optimal LDA classifier was 0.393 ± 0.013, i.e. the scheme proposed in Senn *et al*. (2006) closely achieves the best classification error attainable with linear separation of the subjectively scored dataset. When a 10-fold cross validation experiment was performed on the objectively measured dataset produced by the plug-in, the classification error with the optimal LDA classifier was 0.363 ± 0.021. This error measure is significantly different from the one achieved with the subjective data. However, it should be noted that the difference between the two classification errors is not large.

Discussion

To determine the quality of zygotes we need a non-invasive tool for a quick, precise and reproducible analysis that does not interfere with the daily clinical work in the IVF laboratory. Analysis of images instead of direct microscopic evaluation of zygotes avoids a long exposure of zygotes to a deleterious environment outside the incubator. We have previously shown that subjective scoring of zygote images is feasible and allows the identification of zygotes with high probability to implant (Senn *et al*., 2006). However, the number of analysed features was limited to six, and discrete scores, instead of continuous variables, were assigned to each feature. To increase the number of analysed features and to improve precision in their evaluation, we developed a software tool so as to obtain a morphological fingerprint of individual human zygotes. The plug-in of ImageJ presented in this article provides precise and reproducible measurements of a high number of variables on digital images of zygotes observed under Hoffman modulation contrast.

Images coming from two different IVF laboratories were successfully analysed with the plug-in, indicating that this tool could be used in different laboratories. The average size of the zygotes (mean diameter, 110 μm), measured by the plug-in, was close to the value of 115.9 μm that was measured by Roux *et al*. (Roux *et al*., 1995). The mean diameter of the two PN measured by the plug-in (pronucleus 1: 25 μm, pronucleus 2: 24.4 μm) were similar to the mean values of 27.3 μm and 25.6 μm reported by Roux *et al*. (Roux *et al*., 1995) and to the range values of 16.5–24.1 μm and 15.3–22.4 μm reported by Payne *et al*. (Payne *et al*., 1997). The measurements were similar for the images provided by Group I and by Group II, except for some features. When subjectively scored, the size of the cytoplasmic halo was the only feature significantly different between the two groups. Computer-assisted measurements revealed significant differences between Group I and Group II, not only in the cytoplasmic halo but also in PN centring, PN proximity and NPB distribution. This indicates that computer-assisted analysis is mainly in accordance to subjective scoring but results in better precision in evaluating the zygote features. Therefore, subtle differences between zygotes, not detected by subjective scoring, appear clearly significant after objective measurements. Differences observed between the zygotes from Group I and Group II are probably explained by the differences in the zygote selection policy between the two centres. In the Group II, the transferred embryos, selected on the basis of their quality, originated certainly from zygotes presenting morphological characteristics representative of a high developmental competence. For example, a strongly polarized distribution of NPB observed in zygotes of Group II is considered as a predictor of a good embryo development (Scott, 2003). A lower halo size in Group II compared with Group I zygotes is consistent with the observation that an extreme halo impairs embryo development (Zollner *et al*., 2002). Although the influence of the age of the women and culture conditions (culture system and culture medium) on zygote morphology cannot be excluded in the present study, zygote scores were previously shown to be independent of age (Scott *et al*., 2000) and the influence of culture conditions have not been described as yet.

Identifying zygotes with high implantation probability remains a challenge to improve IVF treatment efficiency while decreasing the occurrence of multiple pregnancies. Prediction of implantation is limited when the only criteria rely on subjective assessment of zygote morphology (Montag and van der Ven, 2001; Zollner *et al*., 2002; Senn *et al*., 2006; Guerif *et al*., 2007), and a number of additional studies have questioned the efficiency of PN scoring for identifying embryos with high implantation potential (James *et al*., 2006;

Arroyo *et al*., 2007; Nicoli *et al*., 2007). The performance of a prognostic test in terms of implantation prediction is demonstrated by its ability to correctly classify most of the analysed zygotes, implying a minimal error rate of classification. In the present study, the classification error averaged 0.39 when using a subjective zygote scoring, which is far from optimal. The computer-assisted measurement of a large number of zygote parameters did not result in a dramatic improvement of classification (error rate 0.36), indicating that the low predictive performance of zygote morphology is probably not due to its imprecise evaluation. This is consistent with a recent statement that prediction of implantation on the basis of zygote morphology is limited, unless it is combined to other relevant parameters describing embryo development (Guerif *et al*., 2007). However, in countries where embryo characteristics cannot be taken in account for embryo selection, PN zygote morphology remains a valuable tool.

In summary, we show that the morphological features extracted by our plug-in can be used for an objective zygote characterization in terms of morphology. It presents the important advantage over the subjective scoring scheme previously proposed in Senn *et al*. (2006) to be totally reproducible. It could therefore contribute to improve the consensus between laboratories on how to evaluate human PN zygotes.

Acknowledgements

The authors thank Serono for their support, and especially Dr Veronica Alam. The authors also thank Dr Marysa Emery for the revision of the manuscript.

Funding

Partial support is acknowledged to Merck-Serono (special thanks are given to Dr. Veronica Alam and Dr. Véronique Moy). Partial support is also acknowledged to Univ. San Pablo CEU through project 04/05.

References

Arroyo G, Veiga A, Santalo J, Barri PN. Developmental prognosis for zygotes based on pronuclear pattern: Usefulness of pronuclear scoring. *J Assist Reprod Genet* 2007;**24**:173–181.

Ebner T, Moser M, Sommergruber M, Tews G. Selection based on morphological assessment of oocytes and embryos at different stages of preimplantation development: a review. *Hum Reprod Update* 2003;**9**:251–262.

Fitzgibbon A, Plu M, Fisher RB. Direct least square fitting of ellipses. *IEEE Trans Pattern Anal Mach Intell* 1999;**21**:476–480.

Gardner DK, Vella P, Lane M, Wagley L, Schlenker T, Schoolcraft WB. Culture and transfer of human blastocysts increases implantation rates and reduces the need for multiple embryo transfers. *Fertil Steril* 1998;**69**:84–88.

Garello C, Baker H, Rai J, Montgomery S, Wilson P, Kennedy CR, Hartshorne GM. Pronuclear orientation, polar body placement, and embryo quality after intracytoplasmic sperm injection and in-vitro fertilization: further evidence for polarity in human oocytes? *Hum Reprod* 1999;**14**:2588–2595.

Germond M, Senn A. A law affecting medically assisted procreation is on the way in Switzerland. *J Assist Reprod Genet* 1999;**16**:341–343.

Gianaroli L, Magli MC, Ferraretti AP, Lappi M, Borghi E, Ermini B. Oocyte euploidy, pronuclear zygote morphology and embryo chromosomal complement. *Hum Reprod* 2007;**22**:241–249.

Guerif F, Le Gouge A, Giraudeau B, Poindron J, Bidault R, Gasnier O, Royere D. Limited value of morphological assessment at days 1 and 2 to predict blastocyst development potential: a prospective study based on 4042 embryos. *Hum Reprod* 2007;**22**:1973–1981.

Hoffman R, Gross L. Reflected-light differential-interference microscopy: principles, use and image interpretation. *J Microsc* 1970;**91**:149–172.

Illingworth J, Kittler J. A survey of the hough transform. *Comput Vis Graph Image Process* 1988;**44**:87–116.

Jain AK. *Fundamentals of Digital Image Processing*. Prentice-Hall, 1989.

James AN, Hennessy S, Reggio B, Wiemer K, Larsen F, Cohen J. The limited importance of pronuclear scoring of human zygotes. *Hum Reprod* 2006;**21**:1599–1604.

Montag M, van der Ven H. Evaluation of pronuclear morphology as the only selection criterion for further embryo culture and transfer: results of a prospective multicentre study. *Hum Reprod* 2001;**16**:2384–2389.

Murphy D. *Fundamentals of Light Microscopy and Electronic Imaging*. Wiley-Liss, 2001.

Nicoli A, Valli B, Di Girolamo R, Di Tommaso B, Gallinelli A, La Sala GB. Limited importance of pre-embryo pronuclear morphology (zygote score) in assisted reproduction outcome in the absence of embryo cryopreservation. *Fertil Steril* 2007;**88**:1167–1173.

Payne D, Flaherty SP, Barry MF, Matthews CD. Preliminary observations on polar body extrusion and pronuclear formation in human oocytes using time-lapse video cinematography. *Hum Reprod* 1997;**12**:532–541.

Roux C, Joanne C, Agnani G, Fromm M, Clavequin MC, Bresson JL. Morphometric parameters of living human in-vitro fertilization embryos; importance of the asynchronous division process. *Hum Reprod* 1995;**10**:1201–1207.

Scott L. Pronuclear scoring as a predictor of embryo development. *Reprod Biomed Online* 2003;**6**:201–214.

Scott L, Alvero R, Leondires M, Miller B. The morphology of human pronuclear embryos is positively related to blastocyst development and implantation. *Hum Reprod* 2000;**15**:2394–2403.

Senn A, Urner F, Chanson A, Primi MP, Wirthner D, Germond M. Morphological scoring of human pronuclear zygotes for prediction of pregnancy outcome. *Hum Reprod* 2006;**21**:234–239.

Shoukir Y, Campana A, Farley T, Sakkas D. Early cleavage of in-vitro fertilized human embryos to the 2-cell stage: a novel indicator of embryo quality and viability. *Hum Reprod* 1997;**12**:1531–1536.

Tesarik J, Greco E. The probability of abnormal preimplantation development can be predicted by a single static observation on pronuclear stage morphology. *Hum Reprod* 1999;**14**:1318–1323.

Unser M, Aldroubi A, Eden M. B-Spline signal processing: Part II– Efficient design and applications. *IEEE Trans Signal Process* 1993;**41**:834–848.

Webb AR. *Statistical Pattern Recognition*. New York: John Wiley and Sons, 2002.

Zollner U, Zollner KP, Hartl G, Dietl J, Steck T. The use of a detailed zygote score after IVF/ICSI to obtain good quality blastocysts: the German experience. *Hum Reprod* 2002;**17**:1327–1333.

Submitted on November 9, 2007; resubmitted on February 7, 2008; accepted on March 21, 2008